

# Transition From Ideal To Viscous Mach Cones In A Kinetic Transport Approach

I. Bouras,<sup>1</sup> A. El,<sup>1</sup> O. Fochler,<sup>1</sup> H. Niemi,<sup>2</sup> Z. Xu,<sup>3</sup> and C. Greiner<sup>1</sup>

<sup>1</sup>*Institut für Theoretische Physik, Johann Wolfgang Goethe-Universität,  
Max-von-Laue-Str. 1, D-60438 Frankfurt am Main, Germany*

<sup>2</sup>*Department of Physics, P.O. Box 35 (YFL) FI-40014 University of Jyväskylä, Finland*

<sup>3</sup>*Department of Physics, Tsinghua University, Beijing 100084, China*

(Dated: July 19, 2022)

Using a microscopic transport model we investigate the evolution of conical structures originating from the supersonic projectile moving through the hot matter of ultrarelativistic particles. Using different scenarios for the interaction between projectile and matter, and different transport properties of the matter, we study the formation and structure of Mach cones. Especially, a dependence of the Mach cone angle on the details and rate of the energy deposition from projectile to the matter is investigated. Furthermore, the two-particle correlations extracted from the numerical calculations are compared to an analytical approximation. We find that the propagation of a high energetic particle through the matter does not lead to the appearance of a double peak structure as observed in the ultrarelativistic heavy-ion collision experiments. The reason is the strongly forward-peaked energy and momentum deposition in the head shock region. In addition, by adjusting the cross section we investigate the influence of the viscosity to the structure of Mach cones. A clear and unavoidable smearing of the profile depending on a finite ratio of shear viscosity to entropy density is clearly visible.

## I. INTRODUCTION

Results from the relativistic Heavy Ion Collider (RHIC) [1] and recently from the Large Hadron Collider (LHC) [2] indicate the formation of a new state of matter, the quark-gluon plasma (QGP). The large value of the measured elliptic flow coefficient  $v_2$  indicates the nearly perfect fluid behaviour of the QGP [3]. This is confirmed by recent calculations of viscous hydrodynamics [4] and microscopic transport calculations [5] with a shear viscosity over entropy density ratio  $\eta/s = 0.1 - 0.2$ , which is close to the conjectured lower bound  $\eta/s = 1/4\pi$  from a correspondence between conformal field theory and string theory in an Anti-de-Sitter space [6].

Highly energetic partons propagating through the hot and dense QGP rapidly lose their energy and momentum as the energy is deposited in the medium. This phenomenon is known as jet-quenching [7, 8], whereas its exact mechanism is still to be fully understood. Furthermore, recent measurements of two- and three-particle correlations in heavy-ion collisions (HIC) show a complete suppression of the away-side jet, whereas for lower  $p_T$  a double peak structure is observed in the two-particle correlation function [9]. For a while one possible and promising origin of these structures was assumed to be the interaction of fast partons with the soft matter which generates collective motion of the medium in form of Mach cones. [10, 11]. In contrast, recent studies of triangular flow from initial fluctuations [12] show a more satisfactory explanation for the appearance of the double peak structure.

The recent idea is that both Mach cones and triangular flow from initial fluctuations exist in heavy-ion collisions, but it is difficult to separate their effects and the two-particle correlations do not seem to be a good observable for this purpose. In the present study we claim that even

if there are no effects from initial stage fluctuations, a double-peak structure in two-particle correlations cannot be expected from the energy-momentum deposition by a jet into the medium. This will be not only due to the viscous effects, but also due to the details of the "Mach cone"-like structure, which was found in a similar form in ideal fluid [13] and AdS/CFT[14] studies.

For this purpose we investigate the propagation and formation of Mach cones in the microscopic transport model BAMPS (Boltzmann Approach of MultiParton Scatterings) [15] in the limit of vanishing mass and very small shear viscosity over entropy density ratio  $\eta/s$  of the matter. Two different scenarios for the jet are used and the dependence of the Mach cone angle on the details of energy deposition is discussed. A simple analytic relation for the expected particle distribution in the Mach cone wings is derived and is compared it to numerical results extracted from BAMPS. In addition, by adjusting  $\eta/s$ , the influence of the viscosity on the profile of the Mach cone and the corresponding two-particle correlation is explored for the first time. In this work the units are  $\hbar = c = k = 1$ . The metric tensor is  $g^{\mu\nu} = \text{diag}(1, -1, -1, -1)$ .

## II. SHOCK WAVES AND MACH CONES

Shock waves are phenomena which have their origin in the collective motion of matter. In the limit of a perfect fluid with no viscosity, a signal caused by a weak perturbation propagates with the speed of sound  $c_s = \sqrt{dp/de}$ , which depends on the equation of state (EOS) of the medium. Here,  $p$  is the equilibrium pressure and  $e$  is the energy density in the local rest frame (LRF). A larger perturbation results in a shock wave propagating faster than the speed of sound. In a simplified one-dimensional

setup shock waves have already been studied for the perfect fluid limit [16]. Furthermore, the viscous solutions have been investigated in Refs. [17, 18], demonstrating that the shock profile is smeared out when viscosity is large. It was also found that a clear observation of the shock within the short time available in heavy-ion collisions requires a small viscosity. The information taken from these studies can be transferred to the investigation of conical shock structures like Mach cones, which is the main subject of this paper.

First, we consider a weak perturbation moving with the speed of light, i.e.  $v_{\text{source}} = 1$ , through the medium of a perfect fluid. For simplification we use a massless relativistic gas with  $e = 3p$  and  $c_s = 1/\sqrt{3}$ . The perturbation generates waves propagating through the medium with the speed of sound  $c_s$ . In this case the propagating modes are called sound waves. If the perturbation moves faster than the speed of sound the created sound waves accumulate on a cone [19]. In the following we refer to the surface of this cone as the shock front.

The resulting emission angle of this shock front relative to the direction of the projectile is given by the weak perturbation Mach angle  $\alpha_w = \arccos(c_s/v_{\text{source}}) = \arccos(1/\sqrt{3}) = 54, 73^\circ$ . It is important to know that in nature perturbations are not sufficiently small. In this case, shock waves instead of sound waves are generated and due to different propagation velocities of these waves, we expect a change of the Mach angle [20]. We can generalize the introduced Mach angle to the case of stronger perturbations:

$$\alpha = \arccos(v_{\text{shock}}/v_{\text{source}}). \quad (1)$$

We require here  $v_{\text{source}} > v_{\text{shock}}$ , where  $v_{\text{shock}}$  is the velocity of the shock front propagating through the medium. The velocity of the shock front depends on the pressure (energy density) on the cone  $p_{\text{cone}}$  ( $e_{\text{cone}}$ ) and the medium itself  $p_{\text{med}}$  ( $e_{\text{med}}$ ) [16]:

$$v_{\text{shock}} = \left[ \frac{(p_{\text{med}} - p_{\text{cone}})(e_{\text{cone}} + p_{\text{med}})}{(e_{\text{med}} - e_{\text{cone}})(e_{\text{med}} + p_{\text{cone}})} \right]^{1/2}. \quad (2)$$

Eq. (2) has the following limits: If  $p_{\text{cone}} \gg p_{\text{med}}$  we obtain  $v_{\text{shock}} = 1$ . If  $p_{\text{cone}} \approx p_{\text{med}}$ , i.e. the perturbation is very weak, we get the expected limit of the speed of sound  $v_{\text{shock}} \approx c_s$ . In the latter case Eq. (1) becomes  $\alpha_w$ , as expected. The collective velocity of matter in the shock wave (Mach cone wing), which is different from the signal propagation velocity (2), can be calculated via

$$v_{\text{coll}} = \left[ \frac{(p_{\text{cone}} - p_{\text{med}})(e_{\text{cone}} - e_{\text{med}})}{(e_{\text{med}} + p_{\text{cone}})(e_{\text{cone}} + p_{\text{med}})} \right]^{1/2}. \quad (3)$$

In the case of a very weak perturbation the collective velocity of matter vanishes,  $v_{\text{coll}} \approx 0$ , whereas for stronger perturbations  $v_{\text{coll}}$  can increase up to the speed of light.

In Sec. IV we discuss the numerical results from BAMPS and expect a clear dependence of the observed Mach angle on the strength of the perturbation according to Eq. (1), but due to non-linear effects Eq. (1) is merely a good approximation.

### III. PARTICLE MOMENTUM DISTRIBUTION IN THE SHOCK FRONT

In order to understand the origin of the double peak structure induced by "Mach cone"-like structures, which will be discussed in Sec. IV, we derive a simple model of particle emission from the shock front of a Mach cone in a 2-dimensional  $xy$ -plane. We assume two sources modeling the two wings of a Mach cone with a constant temperature  $T$  and collective four-velocity  $u^\mu = \gamma(1, \vec{v})$ , where  $\gamma = 1/\sqrt{1 - v^2}$  is the Lorentz gamma factor. Each source consists of massless particles according to the thermal distribution  $f(\mathbf{x}, \mathbf{p}) = \exp(-u_\mu p^\mu/T)$ , where  $\mathbf{p}^\mu = (E, \vec{p})$  is the particle four-momentum. Choosing the  $x$ -axis to be the symmetry axis of the cone, which is simultaneously the propagation direction of the jet, we can write  $u_\pm^\mu = \gamma(1, v \cos \alpha, \pm v \sin \alpha, 0)$ . The  $\pm$  corresponds to each wing of the cone. We identify  $v = v_{\text{coll}}$  with Eq. (3) as the collective velocity of the matter in the shock wave and  $\alpha$  is the Mach angle defined in Eq. (1). Using the same coordinate system we write for the four-momentum vector  $\mathbf{p}^\mu = p(1, \cos \phi \sin \theta, \sin \phi \sin \theta, \cos \theta)$ .  $\phi$  is the azimuthal angle in the  $xy$  plane and  $\theta$  is the polar angle with the  $z$ -axis.

The distribution function is defined as  $dN(2\pi)^3/(dV d^3p) = f(\mathbf{x}, \mathbf{p})$ , where  $dV d^3p/(2\pi)^3$  is the phase space volume element. We are interested in the particle distribution  $dN/(Nd\phi)$  which can be calculated as an integral over the thermal distribution in a certain volume  $V$  on the Mach cone surface. We use  $d^3p = p^2 dp d\phi d(\cos \theta)$  and write

$$\frac{dN}{Nd\phi} = \frac{V}{N(2\pi)^3} \int_0^\pi d\cos \theta \int_0^\infty p^2 \left( e^{-\frac{u_+^\mu p_\mu}{T}} + e^{-\frac{u_-^\mu p_\mu}{T}} \right) dp. \quad (4)$$

We obtain  $N = 8\pi\gamma T^3 V$  by integrating  $dN/(dV d^3p) = f(\mathbf{x}, \mathbf{p})$  over the entire phase space volume. After the integration of (4) we obtain

$$\frac{dN}{Nd\phi} = \frac{1}{8\pi\gamma^4} \sum_{i=1}^2 \left[ \frac{2 + b_i^2}{(1 - b_i^2)^2} + \frac{3b_i}{(1 - b_i^2)^{5/2}} A \right], \quad (5)$$

where  $A = \pi/2 + \arctan(b_i/\sqrt{1 - b_i^2})$ ,  $b_1 = v \cos(\alpha - \phi)$  and  $b_2 = v \cos(\alpha + \phi)$ .

The most important result taken from Eq. (5) is the non-existent double peak structure for small  $v_{\text{coll}}$ , which is against all expectations resulting from the naive picture of a Mach cone. We will discuss this point in more details in Sec. IV by comparing Eq. (5) to the numerical results. Furthermore, the particle distribution is equivalent to the two-particle correlation, since the angle  $\phi$  is always correlated to the direction of the source, which serves as a "trigger" particle.

#### IV. TRANSITION FROM IDEAL TO VISCOUS MACH CONES IN BAMPS

In the following we study the evolution of "Mach cone"-like structures with different scenarios of the jet-medium interaction by using the parton cascade BAMPS [15] – a microscopic transport model which solves the Boltzmann equation  $p^\mu \partial_\mu f(x, p) = C[f(x, p)]$  for on-shell particles based on stochastic interpretation of transition rates. As was demonstrated in previous works, BAMPS is able to explore a large variety of hydrodynamic phenomena and provides a reliable benchmark for hydrodynamic models [17, 21]. The advantage of BAMPS is its ability to handle arbitrary large gradients for any choice of viscosity. Thus it is possible to investigate the complete transition from ideal to viscous behavior.

In this study we focus on investigation of Mach cone evolution in absence of any other effects - i.e. we neglect such effects as initial fluctuations or expansion, which are however relevant in heavy-ion collisions. For this purpose, the space-time evolution of particles is performed in a static box. We initialize a static uniform medium of massless Boltzmann particles with  $T_{\text{med}} = 400$  MeV, which corresponds to a LRF energy density  $e_{\text{med}} = 16.28 \text{ GeV/fm}^3$ . For simplification, we consider only binary collisions with an isotropic cross section, i.e. a cross section with an isotropic distribution of the collision angle. Furthermore, we keep the mean free path  $\lambda_{\text{mfp}}$  of the medium particles constant in all spatial cells by adjusting the cross section according to  $\sigma = 1/(n\lambda_{\text{mfp}})$ , where  $n$  is the particle density. The related shear viscosity for isotropic binary collisions is given by  $\eta = 0.4 e \lambda_{\text{mfp}}$  [22]. Collisions of particles against box boundaries in  $x$  and  $y$  direction are realized as elastic collisions off a wall; in  $z$ -direction we use periodic boundary conditions. This reduces the problem to two dimensions and therefore decreases the numerical expenses.

We introduce two different sources to investigate the evolution of "Mach cone"-like structures. In the so called pure energy deposition scenario (PED) [13] the source propagates and emits particles according to the thermal distribution  $f(x, p) = \exp(-E/T)$ , so that the energy deposition is isotropic in the LRF of the source. In this scenario on average only energy is deposited to the medium, but no net-momentum. In the second scenario, referred to as JET, a highly energetic massless particle (jet) has only momentum in  $x$ -direction, i.e.  $p_x = E_{\text{jet}}$ . The jet propagates and deposits energy to the medium due to collisions with particles. After each collision, the momentum of the jet is reset to its initial value. The jet-medium cross section is adjusted in such a way that we obtain a specific energy deposition rate. Using this scenario a constant energy and momentum deposition rate is achieved. For both scenarios the sources are initialized at  $t = 0$  fm/c at the position  $x = -0.1$  fm and propagate in  $x$ -direction with  $v_{\text{source}} = 1$ , i.e. with the speed of light. We note the JET scenario is a simplified model

of a jet in heavy-ion physics, whereas the PED scenario vaguely resembles the hot spots studied in [23], but in the form implemented here there is no correspondence to heavy-ion collisions. We expect clear differences between these two scenarios concerning the evolution of the entire system, but also concerning the final distribution of the particles.

##### A. Effect of energy deposition rate

In Fig. 1 we show the results for the PED in the upper panel and JET in the lower panel using three different energy deposition rates into the medium,  $dE/dx = 1, 10$  and  $200 \text{ GeV/fm}$ , in the nearly ideal limit, i.e.  $\eta/s \approx 0.005$ . We note that in general the maximum (minimum) energy density in the simulations is larger (smaller) than the maximum (minimum) of the energy density scales in the Figures. Also the plotted arrow length of the velocity profile is scaled. Both modifications are done to enhance the readability of the Figures.

In both scenarios, PED and JET, we observe a conical structure, but with obvious differences. In the PED case with the isotropic energy deposition, a circle of perturbations propagating in backward direction is visible. This is missing in the JET scenario because of the strong momentum deposition in  $x$ -direction. Another difference is that in the JET scenario a clearly visible head shock, i.e. a shock wave in the front of the jet perpendicular to the direction of the jet, appears. This in turn is missing in the PED scenario. Furthermore, there is a clear difference in the behavior of the matter behind the Mach cones. In the JET case, the projectile induces a diffusion wake, where the matter is flowing in the direction of the projectile. Whereas in the PED scenario an opposite behavior is observed, i.e. there is an anti-diffusion wake where the matter behind the cone is flowing in the backward direction. These observations are in qualitative agreement with the results from ideal hydrodynamics and transport calculations [13?].

Additionally, every scenario is compared to the ideal Mach cone with  $\alpha_w$  for a very weak perturbation shown in Fig. 1. Both scenarios provide evidence that the energy deposition rate of the source influences the Mach angle  $\alpha$  of the wings according to Eq. 1. In both cases the shock front is curved because near the projectile the disturbance of the media is strongest and the shock front moves faster than the speed of sound. Farther away from the projectile a part of the energy of the shock front has already dissipated into the medium and as a result the perturbation gets weaker and approaches a weak perturbation propagating with the speed of sound.

In the JET scenario the energy of the jet  $E_{\text{jet}}$  is 20, 200 and  $20000 \text{ GeV}$  (starting from the left in Fig. 1). For our calculations in the nearly ideal limit the energy of the jet does not play any significant role. The only parameter which matters is the average energy deposition rate. We will mention in Sec. IV B how the value of the

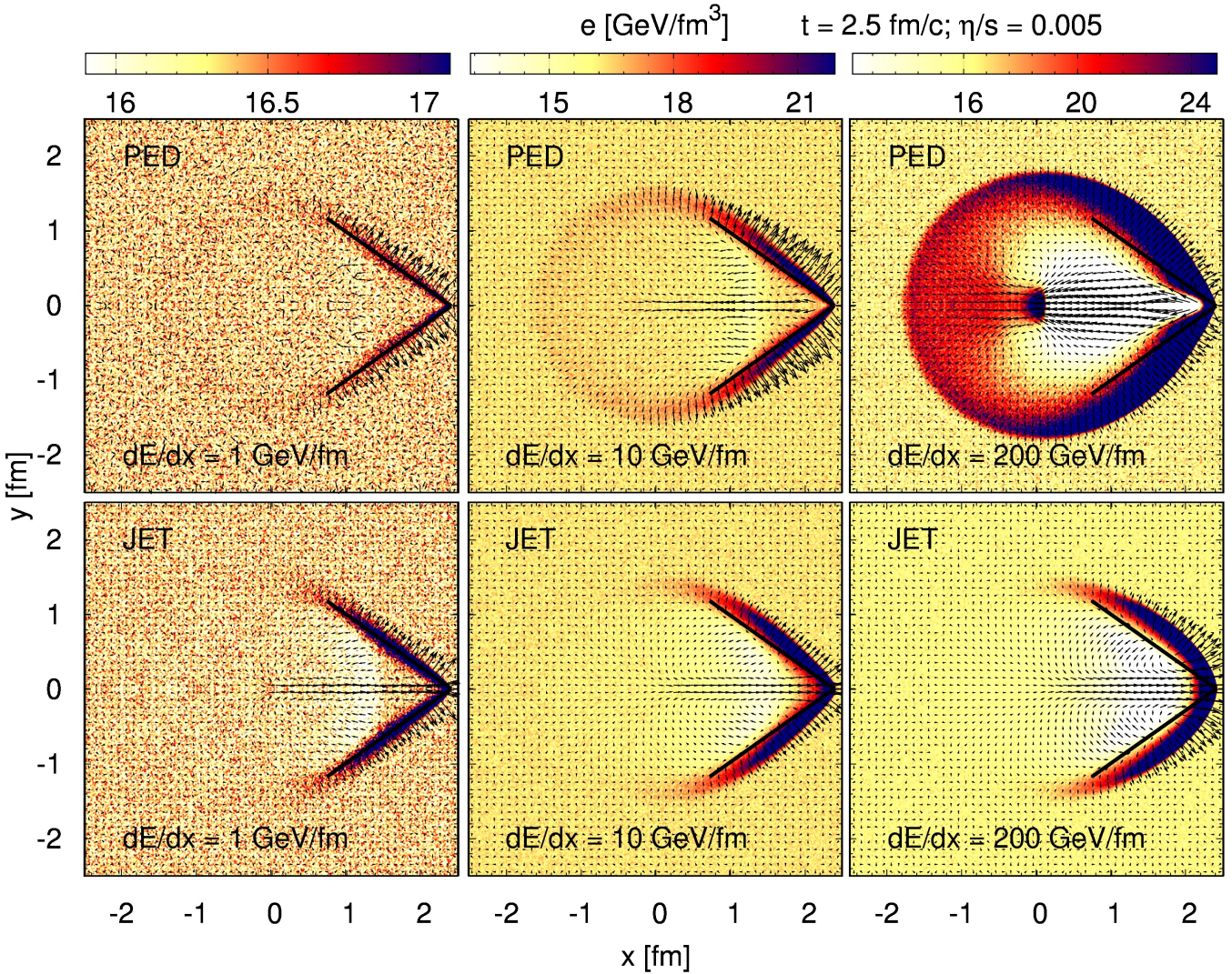


FIG. 1. (Color online) Shape of a Mach cone in the nearly ideal limit ( $\eta/s = 0.005$ ) shown for different jet scenarios and different energy deposition rates into the medium,  $dE/dx = 1, 10$  and  $200$  GeV/fm. The upper panel shows the pure energy deposition scenario (PED); the lower panel shows the propagation of a highly energetic jet (JET) depositing energy and momentum in  $x$ -direction. Depicted are the LRF energy density within a specific range; as an overlay we show the velocity profile with a scaled arrow length. The results are a snapshot of the evolution at  $t = 2.5$  fm/c. In addition we show the analytical solution for the ideal Mach cone in the very weak perturbation case with the emission angle  $\alpha_w$ .

jet energy  $E_{\text{jet}}$  and finite viscosity in the medium changes the pattern of the Mach Cone.

We now want to address the question whether the Mach cone structures observed in Fig. 1 can be regarded as the source of a double peak structure in two-particle correlations. For this purpose we extract the particle distribution  $dN/(Nd\phi)$  from BAMPS calculations. In Fig. 2 (a) we show the results for the energy deposition rate  $dE/dx = 10$  GeV/fm together with the analytical calculation using Eq. (5). To extract only the contribution from the wings and to exclude of all other regions such as (anti-)diffusion wake and back region (especially in the PED scenario), a lower energy density cut at  $20$  GeV/fm $^3$  is applied. Particles in cells with energy

density lower than this value are not considered in the extracted particle distribution (we note that particles from the medium in rest automatically do not contribute to the final profile). For the analytical solution taken from Eq. (5) we use  $e_{\text{cone}} = 22.15$  GeV/fm $^3$  and  $v_{\text{coll}} = 0.137$  ( $e_{\text{cone}}$  represents the average energy density on the Mach Cone wings extracted from the associated numerical calculations). In both scenarios, PED and JET, as well as in the analytical calculation we observe only a peak in the direction of the source, but no double peak structure. This finding is against all expectations from the naive picture of a Mach cone.

However, with a sufficiently higher energy deposition rate the final picture changes significantly. In Fig. 2 (b)

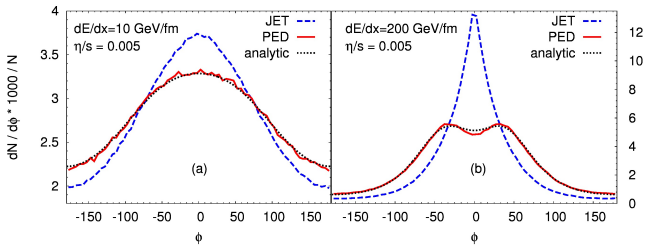


FIG. 2. (Color online) Two particle correlations  $dN/(Nd\phi)$  extracted from calculations shown in Fig. 1. The results are extracted from calculations with  $dE/dx = 10$  GeV/fm (a) and  $dE/dx = 200$  GeV/fm (b). Analytic solutions extracted from Eq. (5) are shown for  $e_{\text{cone}} = 22.15$  GeV/fm $^3$  (a) and  $e_{\text{cone}} = 62.55$  GeV/fm $^3$  (b).

the results from BAMPS calculations with  $dE/dx = 200$  GeV/fm are shown. The lower energy density cut is increased to 50 GeV/fm $^3$  because of the much higher energy deposition rate. For the analytic calculation  $e_{\text{cone}} = 62.55$  GeV/fm $^3$  with  $v_{\text{coll}} = 0.537$  is selected. In the PED scenario, as well as in the analytic model, the double peak structure finally appears as long as the energy deposition rate and consequently  $v_{\text{coll}}$  are sufficiently large. However, in the JET scenario only a peak in the direction of the jet is visible.

We want to mention that in the PED scenario using special momentum cuts (not considered in this work), i.e. restricting the momentum integration in Eq. (5) to a certain interval one can always obtain a double peak in the distribution. However, in the JET scenario a double peak never appears, regardless of momentum cuts.

There are two main contributions to the structure of the two-particle correlation, one from the wings of the Mach cone and one from the head shock region. The matter in the wings is moving in the direction perpendicular to the surface with some collective velocity  $v_{\text{coll}}$ . The larger the collective velocity, the more strongly peaked are the local particle distribution functions into this direction. From our simple analytic model it is clear that the mere existence of the wings is not enough to have clearly visible peaks in the correlation, but the local velocity of the matter has to be sufficiently large. This is also confirmed by the full simulations: If the energy deposition rate is sufficiently large in the PED scenario, the double peaks appear.

In principle, the same reasoning also works for the JET scenario. However, in this case there is also a strong contribution from the head shock region, where the matter is moving with large collective velocity. This collective motion is in the direction of the projectile and results in a particle distribution function that is peaked in the same direction. Although a double peak due to the Mach cone wings still exists, the contribution of the head shock clearly dominates and overshadows the contribution from the wing regions (with spatial cuts to remove the head shock the double peak appears again [11]). Thus, no

double peaks appear in the JET scenario.

## B. Effects of viscosity

In Fig. 3 we show the Mach Cone structure for both PED scenario (upper panel) and JET scenario (lower panel) with  $\eta/s = 0.005, 0.05, 0.2$  and  $0.5$  from left to right, respectively. The energy deposition rate is fixed to  $dE/dx = 200$  GeV/fm. In addition,  $E_{\text{jet}} = 20000$  GeV is used in the JET scenario. The chosen  $\eta/s$  values are intended to cover the nearly-ideal limit (0.005), the estimated QGP shear viscosity over entropy density ratio in heavy-ion collisions (0.05, 0.2)[4, 5] and highly viscous limit where dissipative hydro calculations are not reliable anymore (0.5) [17].

First, we note that if we observe the system at fixed time, then in both scenarios the Mach cone structure smears out and eventually disappears almost completely as the viscosity increases. This is true for shock fronts as well as for the (anti-) diffusion wake. The difference between the PED and the JET case is that as  $\eta/s$  increases, in the PED scenario the resulting "Mach cone" solution covers approximately the same spatial region regardless of a value of  $\eta/s$ , while in the JET case the structure is concentrated more and more near the projectile as the viscosity increases. The reason for this is that in the PED scenario the momentum from the projectile is isotropically deposited into the medium, while in the JET scenario the initial momentum dissipation is strongly peaked into the direction of the projectile (the effect in the JET scenario becomes even stronger with increasing energy of the jet  $E_{\text{jet}}$ , since scattered the particles are stronger forward-peaked). With a large viscosity the re-scattering of the emitted particles from the source is very rare. Thus, the larger the viscosity the more the resulting solution reflects the details of the projectile-matter interaction.

We note that in both scenarios the projectiles are point-like and initially the matter is homogeneously distributed. Therefore, as long as we keep the energy dissipation rate constant, the only length scale that controls the solution is the mean free path  $\lambda_{\text{mfp}} \propto \eta$ . Thus, we expect a similar scaling behavior as in the one-dimensional Riemann problem [17]. For example, the energy density profiles for two different shear viscosities  $\eta$  and  $\eta'$  are related by

$$e(t - t_0, x - x_0, y - y_0, \eta') = e\left(\frac{t - t_0}{C}, \frac{x - x_0}{C}, \frac{y - y_0}{C}, \eta\right), \quad (6)$$

where the scaling factor  $C = \eta'/\eta$ , and  $x_0$  and  $y_0$  are the coordinates of the projectile at the time  $t_0$ .

Using this scaling behavior, we can also read Fig. 3 as a time-evolution of the solution, with a larger viscosity corresponding an earlier time. For example, the solutions with  $\eta/s = 0.5$  in the right-most panel of Fig. 3 will evolve to the ones with  $\eta/s = 0.05$  at time  $t = 25$  fm/c

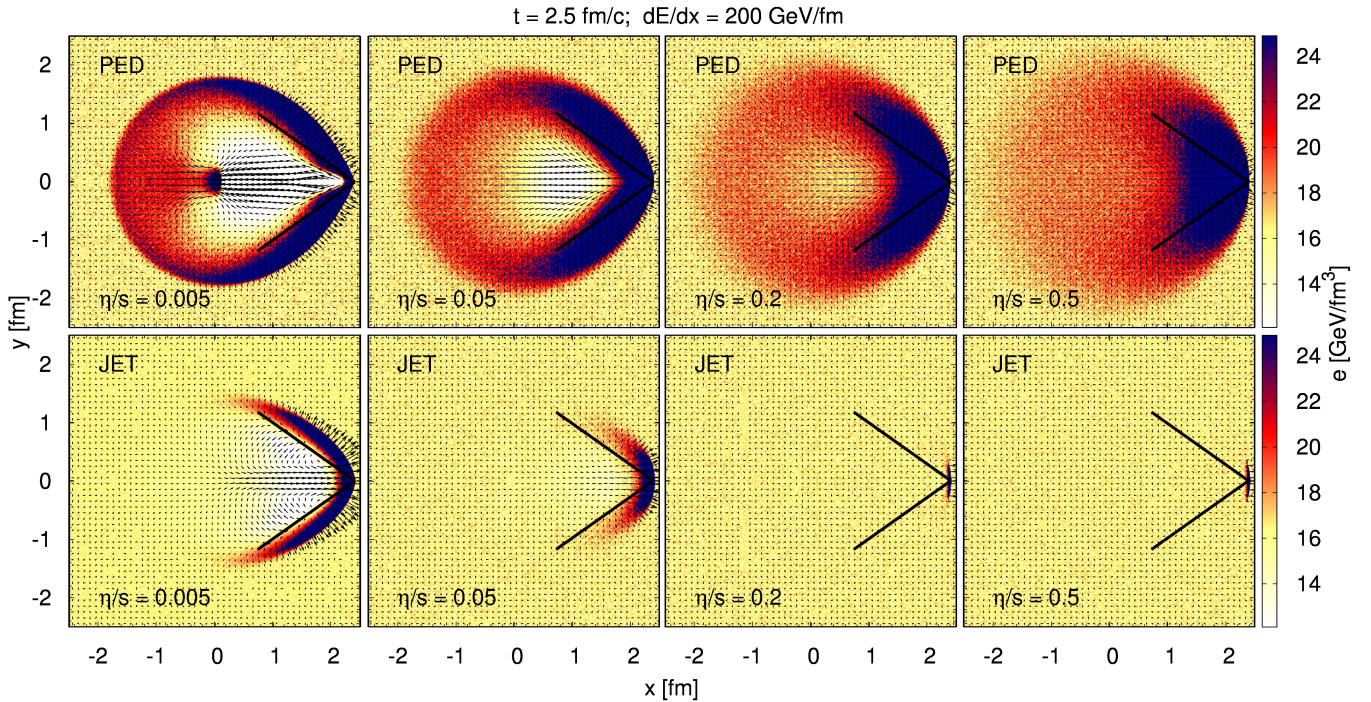


FIG. 3. (Color online) Transition from ideal to viscous Mach cones. Shape of a Mach cone shown for different jet scenarios and different viscosity over entropy density ratios,  $\eta/s = 0.005, 0.05, 0.2$  and  $0.5$ . The energy deposition is  $dE/dx = 200$  GeV/fm. The upper panel shows the pure energy deposition scenario (PED); the lower panel shows the propagation of a highly energetic jet (JET) depositing energy and momentum in  $x$ -direction. Depicted are the LRF energy density within a specific range; as an overlay we show the velocity profile with a scaled arrow length. The results are a snapshot of the evolution at  $t = 2.5$  fm/c. In addition we show the analytic solution for the ideal Mach cone in the very weak perturbation case with the emission angle  $\alpha_w$ .

(with the appropriate scaling of the  $x$ - and  $y$ -axis). Although, from Fig. 3 the Mach angle apparently changes with the viscosity, this is a transient effect related to a finite formation time of the Mach cone with non-zero viscosity. The viscosity affects the width and formation time of the shock front, but not its speed of propagation, i.e. the relation (2) still holds for non-zero viscosity. Asymptotically, the Mach cone angle will be the same regardless of the value of  $\eta/s$ .

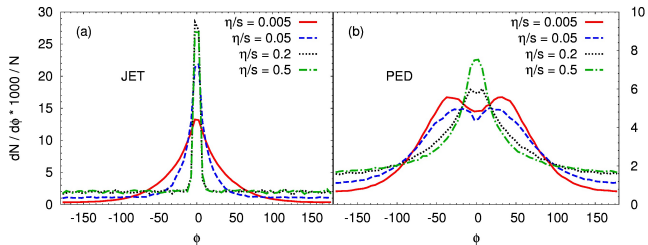


FIG. 4. (Color online) Two particle correlations  $dN/(Nd\phi)$  for different viscosities extracted from calculations shown in Fig. 3. The results are shown in the for the JET (a) and PED (b) scenario for  $dE/dx = 200$  GeV/fm.

In Fig. 4 we show the two-particle correlations for the solutions from Fig. 3. The procedure is similar to the

one discussed for Fig. 2. The lower energy density cut is chosen to be 50 GeV/fm<sup>3</sup>. For the JET scenario (a), the peak in direction of the jet becomes sharper with larger viscosity and no other appreciable effect originating from viscosity is visible. In contrast, for the PED scenario (b) the viscosity destroys the double peak structure. If the viscosity is very large, only a peak in direction of the jet is visible. As above, these results can also be read as a time-evolution of the solution. Fig. 4 shows how the angular distribution of the emitted particles widens with time, or equivalently with increasing  $\eta/s$ .

## V. CONCLUSIONS

In summary, we have investigated the structure of relativistic Mach cones by using a microscopic transport model. The simulations were realized by using two different types of sources propagating through the matter, the PED and JET scenarios. The effect of the strength of the projectile-matter interaction was studied by varying the energy dissipation rate from the projectile to the matter. Furthermore, the effect of the viscosity of the matter was investigated by adjusting the shear viscosity over entropy density ratio  $\eta/s$  from 0.005 to 0.5.

We observed the conical structures form for both types

of sources in the nearly perfect fluid limit, similar to observations in [13], with the Mach Cone angle depending on the energy dissipation rate. We also demonstrated that the non-vanishing viscosity tends to destroy the clear conical structure. By using a scaling of the solutions, we argued that increasing the viscosity has the same effect as looking at the solution at an earlier time. The larger the viscosity or, equivalently, the less time the Mach cone has to develop, the more the structure of the solution depends on the details of the projectile-matter coupling.

Although Mach cone-like structures are observed in BAMPS calculations for different energy and momentum deposition scenarios they are not necessarily associated with double peak structures in the azimuthal particle distributions in  $dN/(Nd\phi)$ . We found that only the PED scenario together with a rather high energy deposition rate lead to a double peak structure, which otherwise cannot be observed because of the strong diffusion wake and head shock. However, the PED scenario has no correspondence in heavy-ion physics. On the other hand, the JET scenario is a simplified model but nevertheless

less demonstrates that a double peak structure cannot be produced by jets with energy and momentum deposition. We expect that our conclusions will still be valid for realistic jets and energy loss scenarios [24]. In addition, a clear Mach cone structure, which is necessary but not in itself sufficient to produce a double peak structure in two-particle correlations, will hardly develop in a system of the size and finite viscosity relevant for HIC. We thus conclude that the double peak structure is not the appropriate observable for the signal of Mach cones in heavy-ion collision experiments.

The authors are grateful to F. Reining, E. Molnar, B. Betz, J. Noronha, G. Torrieri, P. Huovinen, J. Ulery, P. Rau and H. Stöcker for discussions and to the Center for Scientific Computing (CSC) at Frankfurt University for the computing resources. IB is grateful to HGS-Hire. The work of H. Niemi was supported by the Extreme Matter Institute (EMMI). This work was supported by the Helmholtz International Center for FAIR within the framework of the LOEWE program launched by the State of Hesse.

---

[1] I. Arsene *et al.* [BRAHMS Collaboration], Nucl. Phys. A **757**, 1 (2005). K. Adcox *et al.* [PHENIX Collaboration], Nucl. Phys. A **757**, 184 (2005). B. B. Back *et al.*, Nucl. Phys. A **757**, 28 (2005). J. Adams *et al.* [STAR Collaboration], Nucl. Phys. A **757**, 102 (2005).

[2] K. Aamodt *et al.* [The ALICE Collaboration], arXiv:1011.3914 [nucl-ex].

[3] S. S. Adler *et al.* [PHENIX Collaboration], Phys. Rev. Lett. **91**, 182301 (2003); J. Adams *et al.* [STAR Collaboration], *ibid.* **92**, 052302 (2004); B. B. Back *et al.* [PHOBOS Collaboration], Phys. Rev. C **72**, 051901 (2005). A. D. f. Collaboration, arXiv:1107.0454 [nucl-ex]. R. A. Lacey, A. Taranenko, N. N. Ajitanand and J. M. Alexander, Phys. Rev. C **83**, 031901 (2011) [arXiv:1011.6328 [nucl-ex]].

[4] M. Luzum and P. Romatschke, Phys. Rev. C **78**, 034915 (2008); H. Song and U. W. Heinz, J. Phys. G **36**, 064033 (2009). H. Niemi, G. S. Denicol, P. Huovinen, E. Molnar and D. H. Rischke, arXiv:1101.2442 [nucl-th]. B. Schenke, S. Jeon and C. Gale, Phys. Rev. Lett. B **702**, 59 (2011) [arXiv:1102.0575 [hep-ph]].

[5] Z. Xu, C. Greiner and H. Stöcker, Phys. Rev. Lett. **101**, 082302 (2008); Z. Xu and C. Greiner, Phys. Rev. C **79**, 014904 (2009); J. Xu and C. M. Ko, Phys. Rev. C **83**, 034904 (2011) [arXiv:1101.2231 [nucl-th]].

[6] P. Kovtun, D. T. Son and A. O. Starinets, Phys. Rev. Lett. **94**, 111601 (2005) [hep-th/0405231].

[7] J. Adams *et al.* [STAR Collaboration], Phys. Rev. Lett. **91**, 172302 (2003); A. Adare *et al.* [PHENIX Collaboration], *ibid.* **101**, 232301 (2008).

[8] M. Gyulassy and L. McLerran, Nucl. Phys. A **750**, 30 (2005) [arXiv:nucl-th/0405013].

[9] F. Wang [STAR Collaboration], J. Phys. G **30**, S1299 (2004); J. Adams *et al.* [STAR Collaboration], Phys. Rev. Lett. **95**, 152301 (2005); S. S. Adler *et al.* [PHENIX Collaboration], *ibid.* **97**, 052301 (2006); J. G. Ulery [STAR Collaboration], Nucl. Phys. A **774**, 581 (2006); N. N. Ajitanand [PHENIX Collaboration], *ibid.* **783**, 519 (2007); A. Adare *et al.* [PHENIX Collaboration], Phys. Rev. C **78**, 014901 (2008).

[10] H. Stöcker, Nucl. Phys. A **750**, 121 (2005); J. Ruppert and B. Müller, Phys. Lett. B **618**, 123 (2005); J. Casalderrey-Solana, E. V. Shuryak and D. Teaney, J. Phys. Conf. Ser. **27**, 22 (2005); V. Koch, A. Majumder and X. N. Wang, Phys. Rev. Lett. **96**, 172302 (2006). R. B. Neufeld and I. Vitev, arXiv:1105.2067 [hep-ph]. R. B. Neufeld and T. Renk, Phys. Rev. C **82**, 044903 (2010) [arXiv:1001.5068 [nucl-th]]. R. B. Neufeld, B. Müller and J. Ruppert, Phys. Rev. C **78**, 041901 (2008). S. S. Gubser, S. S. Pufu and A. Yarom, Phys. Rev. Lett. **100**, 012301 (2008). J. Noronha, M. Gyulassy and G. Torrieri, Phys. Rev. Lett. **102**, 102301 (2009). G. L. Ma, S. Zhang, Y. G. Ma, H. Z. Huang, X. Z. Cai, J. H. Chen, Z. J. He and J. L. Long *et al.*, “parton/hadron transport model,” Phys. Lett. B **641**, 362 (2006) [nucl-th/0601012]. S. Zhang, G. L. Ma, Y. G. Ma, X. Z. Cai, J. H. Chen, H. Z. Huang, W. Q. Shen and X. H. Shi *et al.*, “correlations for central Au + Au collisions at  $s(\text{NN})^{**}(1/2) = 200\text{-GeV}$ ,” Phys. Rev. C **76**, 014904 (2007) [arXiv:0706.3820 [nucl-th]]. W. Li, S. Zhang, Y. G. Ma, X. Z. Cai, J. H. Chen, H. Z. Huang, G. L. Ma and C. Zhong, “from a multiphase transport model calculation,” Phys. Rev. C **80**, 064913 (2009).

[11] I. Bouras *et al.*, J. Phys. Conf. Ser. **230**, 012045 (2010). I. Bouras *et al.*, J. Phys. Conf. Ser. **270**, 012012 (2011) [arXiv:1008.4072 [hep-ph]].

[12] G. L. Ma and X. N. Wang, Phys. Rev. Lett. **106**, 162301 (2011) [arXiv:1011.5249 [nucl-th]]. B. Schenke, S. Jeon and C. Gale, Phys. Rev. Lett. **106** (2011) 042301 [arXiv:1009.3244 [hep-ph]]. R. S. Bhalerao, M. Luzum and J. Y. Ollitrault, arXiv:1107.5485 [nucl-th].

[13] B. Betz, J. Noronha, G. Torrieri, M. Gyulassy, I. Mishustin and D. H. Rischke, Phys. Rev. C **79**, 034902 (2009) [arXiv:0812.4401 [nucl-th]]. B. Betz, J. Noronha, G. Tor-

rieri, M. Gyulassy, D. H. Rischke, Phys. Rev. Lett. **105**, 222301 (2010). [arXiv:1005.5461 [nucl-th]].

[14] J. Noronha, M. Gyulassy and G. Torrieri, Phys. Rev. Lett. **102**, 102301 (2009) [arXiv:0807.1038 [hep-ph]].

[15] Z. Xu and C. Greiner, Phys. Rev. C **71** (2005) 064901. Z. Xu and C. Greiner, Phys. Rev. C **76**, 024911 (2007).

[16] V. Schneider *et al.*, J. Comput. Phys. **105** (1993) 92;

[17] I. Bouras *et al.*, Phys. Rev. Lett. **103** (2009) 032301 I. Bouras *et al.*, Nucl. Phys. A **830**, 741C (2009) I. Bouras *et al.*, arXiv:1006.0387 [hep-ph].

[18] E. Molnar, Eur. Phys. J. C **60** (2009) 413 [arXiv:0807.0544 [nucl-th]]. M. Mendoza, B. Boghosian, H. J. Herrmann and S. Succi, Phys. Rev. Lett. **105**, 014502 (2010) [arXiv:0912.2913 [physics.plasm-ph]]. D. Hupp, M. Mendoza, I. Bouras, S. Succi and H. J. Herrmann, arXiv:1109.0640 [hep-th].

[19] L. D. Landau and E. M. Lifshitz, Pergamon Press, New York, (1987).

[20] D. H. Rischke, H. Stoecker, W. Greiner, Phys. Rev. **D42**, 2283-2292 (1990).

[21] A. El, I. Bouras, F. Lauciello, Z. Xu, C. Greiner, [arXiv:1103.4038 [hep-ph]].

[22] S. R. de Groot, W. A. van Leeuwen, Ch. G. van Weert, *Relativistic Kinetic Theory: Principles and Applications* North Holland (1980) C. Wesp, A. El, F. Reining, Z. Xu, I. Bouras and C. Greiner, Phys. Rev. C **84**, 054911 (2011) [arXiv:1106.4306 [hep-ph]]. F. Reining, I. Bouras, A. El, C. Wesp, Z. Xu and C. Greiner, arXiv:1106.4210 [hep-th]. A. El, A. Muronga, Z. Xu and C. Greiner, Phys. Rev. C **79**, 044914 (2009) [arXiv:0812.2762 [hep-ph]]. Z. Xu and C. Greiner, Phys. Rev. Lett. **100**, 172301 (2008) [arXiv:0710.5719 [nucl-th]].

[23] J. Takahashi, B. M. Tavares, W. L. Qian, R. Andrade, F. Grassi, Y. Hama, T. Kodama and N. Xu, Phys. Rev. Lett. **103**, 242301 (2009) [arXiv:0902.4870 [nucl-th]]. B. Betz, EPJ Web Conf. **13**, 07002 (2011) [arXiv:1012.4418 [nucl-th]].

[24] O. Fochler, Z. Xu and C. Greiner, Phys. Rev. C **82**, 024907 (2010) [arXiv:1003.4380 [hep-ph]].